Chapter 5

Exploring Pd(0)/g-C_3N_4O Catalyzed Suzuki-Miyaura Cross-Coupling Reaction with Minimal Base-Stoichiometry

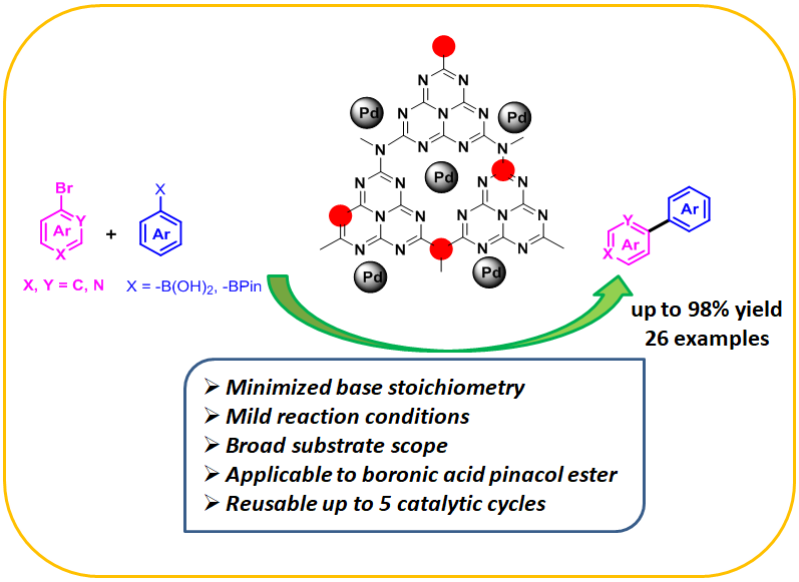

Abstract: Pd nanoparticles (NPs) decorated on a graphitic carbon nitride oxide (g-C_3N_4O) sheet is developed as an efficient heterogeneous catalyst for Suzuki-Miyaura cross-coupling reaction under limiting basic conditions. The developed catalyst, Pd(0)/g-C_3N_4O provides excellent yields of the desired cross-coupled product just under a sub-stoichiometric amount of exogenous base which is the highlight of this work. The graphitic sheet is derived from guanidine hydrochloride and it plays a pivotal role in homogeneous dispersion of Pd NPs, thereby enhancing its catalytic activity. The spectral characteristics of g-C_3N_4O differ significantly from that of g-C_3N_4. The synthesized catalyst is characterized by FT-IR, p-XRD, SEM-EDX, TEM, BET, and XPS analyses. Further, this nanocatalyst is easily recovered from the reaction medium and can be reused for up to five cycles without significant loss of its catalytic activity.

5.1 Introduction

The revolutionary Suzuki-Miyaura (S−M) cross-coupling reaction introduced "green" organoborons as the nucleophilic coupling partner to electrophilic aryl halides for the construction of carbon-carbon (C−C) bonds to access biaryls and functionalized aromatic scaffolds [1]. A conventional S−M cross-coupling is ineffective without a "base" and generally requires about 2-3 equivalents of an inorganic base (usually NaOH, KOH or alkoxides). It is well-understood that the main function of the base in a S−M cross-coupling is to enhance the activity of the arylboronic acid (after the oxidative addition step) towards the transmetallation step with R'−Pd^{II}−X, by forming the corresponding organoborate; R−$B(OH)_3^-$ and resulting in the formation of R'−Pd^{II}−R [2]. Although inorganic bases are commonly employed in this case, they are weakly ionized in organic media which de-accelerates the important transmetallation step [3]. On the other hand, organic bases are comparatively expensive and hygroscopic. To note, base stoichiometry is an important factor while designing the reaction; as the use of an excessive amount of base can alter the acid-base equilibrium and hamper reaction yield [2]. Hence from a sustainability point of view, both "base selection" and "base optimization" are crucial aspects of a S−M cross-coupling reaction.

Another important aspect is the use of Pd metal as catalyst in the reaction. The nature of bulky phosphine ligands used with Pd in the traditional S−M cross-couplings dictates the rate of oxidative addition process of the reaction [4]. However, the increasing challenge of complex substrates and development of sustainable reaction conditions have prompted the design of heterogeneous Pd-catalysts that are easier to handle and facilitates catalyst separation and reusability; particularly the ones supported with Pd(0) NPs [5]. Such catalysts possess the benefit of overcoming the initial dissociative process for the formation of active Pd(0) from the employed Pd(II) pre-catalyst *in situ* [6]. Additionally, Pd(0) NPs are beneficial on account of their high surface area and ability to allow reactions in low catalyst loadings. In this respect, "biosynthesis" of these Pd NPs exerts a sustainability impact to the traditionally developed Pd(0) heterogeneous catalytic systems [7]. Hence, solid-supported Pd NPs catalysts for Suzuki-Miyaura cross-coupling reaction have gained immense attention in recent years.

Researches in recent years have shown that graphitic carbon nitride (g-C_3N_4) is a unique support for metal NPs. It is a two-dimensional polymer with graphite-like layered structure having sp^2 bonded carbon and nitrogen atoms [8]. This sheet acts as a

promising catalytic support due to its chemical and thermal stability, textural property and inexpensive preparation [9]. The high thermal and chemical stability of g-C_3N_4 is due to the extensive π-electron density of C−N heterocycle and van der Waals force within the layers of the sheet [10]. g-C_3N_4 is abundant in nitrogen functionalities, which are the prospective ideal sites for the diverse chemical modifications [11]. The synthesis of g-C_3N_4 can be easily done on a large scale *via* single-step thermal condensation of low-cost suitable precursors having nitrogen atoms such as melamine [12], urea [13], thiourea [14], cyanamide [15], dicyandiamide [16], etc. The functional group modification of g-C_3N_4 with oxygen atom has drawn the attention of researchers in recent years. The substitution of nitrogen by oxygen in the polymeric matrix of g-C_3N_4 is facile and oxygen can occupy some of the nitrogen atoms of the heptazine unit, nitrogen atoms connecting the heptazine units or the surface amine groups and generated g-C_3N_4O sheet contains additional active sites and provides a good dispersion of the oxidized material in water [17]. Also, the electron-rich g-C_3N_4O sheet maintains the required electron density around the metal NPs; which is necessary for a facile oxidative addition step. This electron density is otherwise maintained by the use of costly ligands. The catalytic prospect of g-C_3N_4O has been widely explored in environmental remediation, photo-catalysis, hydrogenation, hydrogen evolution, and singlet oxygen generation [18].

Integrating all the above, in this chapter we demonstrate an unprecedented example of S−M cross-coupling reaction; in which biosynthesized Pd NPs supported on a graphitic carbon nitride oxide surface (Pd(0)/g-C_3N_4O) promotes the reaction in just 0.5 equivalent of an exogenous base providing impressive yields of desired biaryls. The Pd NPs are synthesized with the help of pomegranate (*Punica granatum*) peel extract which acts as a reducing and stabilizing agent for them. The use of pomegranate peel extract as a reducing and stabilizing agent is mainly attributed to the easy availability of the fruit globally [7a]. These peels contain higher polyphenol content (ellagic and gallic acid, ellagic tannins) which reduces and stabilizes the NPs [7a-c]. These metal NPs are dispersed on g-C_3N_4O sheet and are stabilized up to five reaction cycles (Figure **5.1**). The g-C_3N_4O sheet is expected to perform two important functions. First, it directs the aryl halide molecules towards the surface absorbed electron-rich Pd NPs and thus accelerates the oxidative addition step. The aryl halide molecules interact with the π–π stacked layers of g-C_3N_4O and thus remain in close vicinity of the Pd NPs [19]. Second

is the activation of the arylboronic acid. The nucleophilicity of the organoboron can be increased either through its nitrogen lone pairs or through its terminal –OH groups to form the $R-B(OH)_3^-$; thus acting as a pseudo-base and facilitating the overall reaction in minimum equivalents of an exogenous base [20]. The synthesis of the Pd(0)/g-C_3N_4O catalyst is simple and avoids complex multi-step preparation procedures. Moreover, the developed S−M cross-coupling methodology is additive-free and run in an open-flask under aqueous conditions.

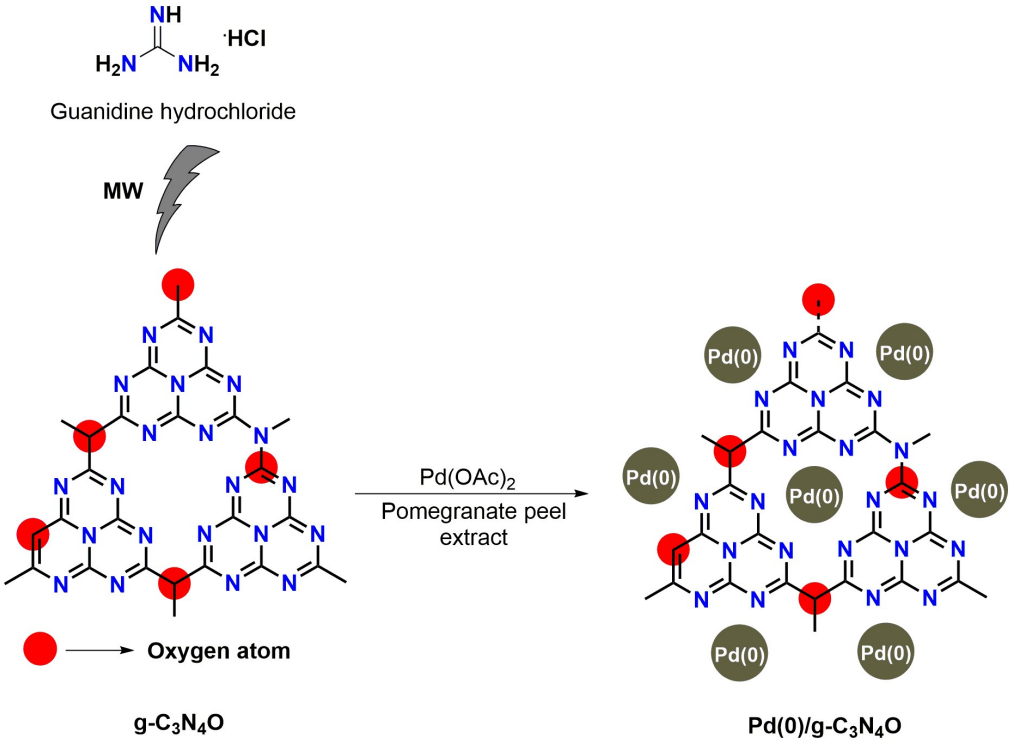

Figure **5.1**. Synthesis of Pd(0)/g-C_3N_4O

5.2 Experimental Section

5.2.1 Synthesis of g-C_3N_4O

g-C_3N_4O was prepared by using guanidine hydrochloride as the precursor material. In our work, we dissolved 0.475 g of guanidine hydrochloride in 10 mL of distilled water by stirring at room temperature in a 250 ml Erlenmeyer flask. To that mixture, 0.5 mL of PEG-400 was added and stirred at room temperature. Then the flask was placed in the microwave at 600W for five minutes and then for another two minutes. After cooling the flask to room temperature, the resulting mixture was then diluted with 50 ml of distilled water. A yellow transparent liquid of g-C_3N_4O was obtained after filtration of the solution.

5.2.2 Synthesis of Pd(0)/g-C_3N_4O

A grounded mass (10 g) of waste pomegranate peels residue was mixed with 100 mL of distilled water. The mixture was filtered and the filtrate (pomegranate peel extract) was collected for further use. 0.050 g of $Pd(OAc)_2$ was mixed with 5 mL of pomegranate peel extract and 5 mL of g-C_3N_4O solution and stirred at room temperature. After 2-3 days, the colour of the solution changed from brown to black. This mixture was centrifuged, washed with ethanol-water mixture and the residue obtained was dried in a desiccator and directly used as the catalyst for Suzuki-Miyaura cross-coupling reaction.

5.2.3 General procedure for synthesis of biaryls

A mixture of aryl bromide (0.5 mmol), arylboronic acid (0.5 mmol), Pd(0)/g-C_3N_4O (5 wt%), K_2CO_3 (0.25 mmol), and EtOH:H_2O (1:1) (4 mL) were taken in a 50 mL round bottomed flask and stirred at room temperature for 5 hours. After completion of the reaction (monitoring by TLC), the reaction mixture was extracted with ethyl acetate, washed with brine solution, and dried over by anhydrous sodium sulfate. The crude was obtained by evaporating the solvent under reduced pressure in a rotary evaporator. To obtain the desired product, purification of the crude was done by column chromatography using silica gel and hexane:ethyl acetate as solvent system.

5.3 Results and Discussion

5.3.1 Characterization of synthesized materials

The FT-IR spectrum (Figure **5.2a**) for g-C_3N_4O shows a peak at 773 cm^{-1} which corresponds to the characteristic breathing mode of heptazine or tri-*s*-triazine unit confirming the presence of heptazine units in the support material [8,9b]. The shifting of the peak to 773 cm^{-1} compared to 810 cm^{-1} of g-C_3N_4 indicates the incorporation of oxygen moieties in the prepared catalyst [21]. The peak at 942 cm^{-1} can be assigned to the stretching of the C−O−C bond [22]. The series of peaks between 1000-1700 cm^{-1} can be ascribed to the stretching vibrations of C−O, C=O, C−N, and C=N bonds in the heptazine-derived repeating units of both metal-loaded and metal-free forms of g-C_3N_4O [8,22]. The peaks present in the range of 2900-3500 cm^{-1} in the spectra correspond to the stretching vibrational modes of the N−H bond in =NH or $–NH_2$ of uncondensed amino and surface adsorbed O−H groups [9a,17,23]. From the IR spectrum, it is seen that the N−H stretching vibrations decrease after loading of Pd NPs which indicates that the

nitrogen functionalities (=NH and –NH_2) are the anchoring sites for the metal NPs [9a]. The peak at 882 cm^{-1} is attributed to the N−H deformation mode [24]. In p-XRD pattern of g-C_3N_4O (Figure **5.2b**), the sharp peaks at 2θ = 32.1° and 22.4° are due to the π–π stacking of aromatic conjugated system which indicates the strong binding and tight packing of the layers of the sheet [8,9b,21,25]. The presence of oxygen atoms within the layers of the graphitic sheet maintains the planar structure through hydrogen bonding and π–π stacking. After the incorporation of Pd NPs, the intensity of the peaks at 2θ = 32.1°, and 22.4° decreased dramatically which indicates the disturbance in rigid packing of layers of the graphitic sheet [9b]. The sharp peaks at 2θ = 40.1°, 46.5° and 68.1° corresponds to (111), (200) and (220) crystallographic planes of face centred cubic lattice (*fcc*) of Pd with lattice spacing, *d* = 0.225, 0.194 and 0.138 nm, respectively [7a, 26]. This confirms the incorporation of metallic Pd(0) NPs on the g-C_3N_4O surface. The p-XRD data agrees well with the existing references (JCPDS card no. 89-4897).

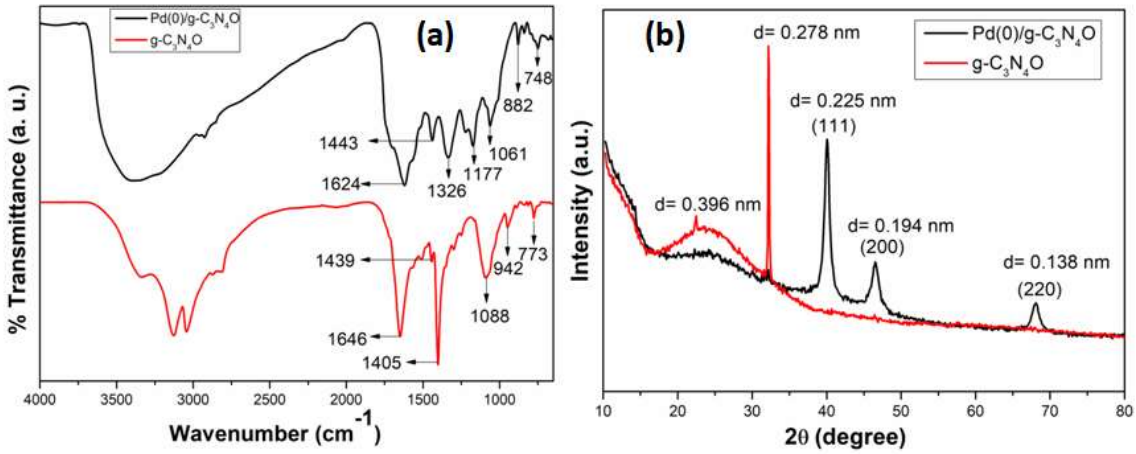

Figure **5.2**. (**a**) FT-IR spectra of g-C_3N_4O (red) and Pd(0)/g-C_3N_4O (black); (**b**) p-XRD pattern of g-C_3N_4O (red) and Pd(0)/g-C_3N_4O (black)

The elemental analysis of Pd(0)/g-C_3N_4O is done with energy dispersive X-ray (EDX) technique (Figure **5.3**), which shows the presence of Pd, C, N, and O along with a trace amount of K and Ca. Further, inductively coupled plasma optical emission spectrometry (ICP-OES) analysis reveals that 1g of solid Pd(0)/g-C_3N_4O contains 16 mg of Pd.

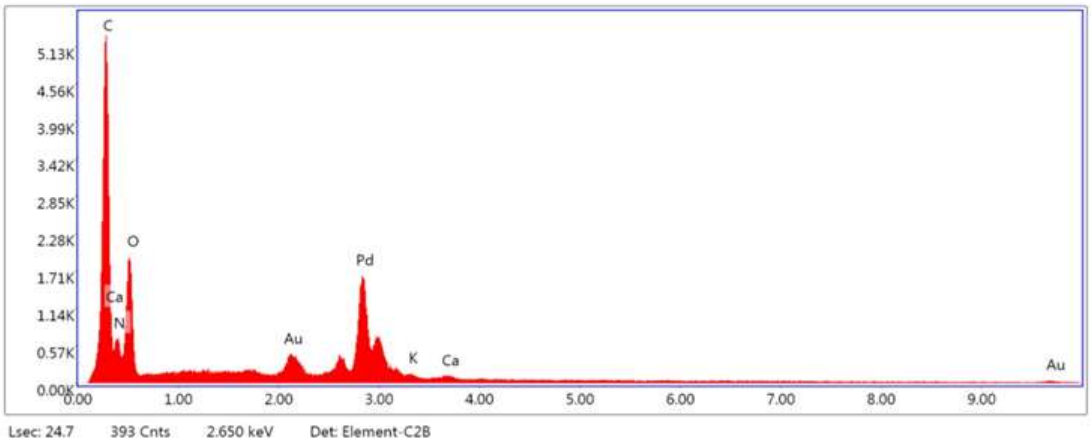

Figure **5.3**. EDX image of Pd(0)/g-C_3N_4O

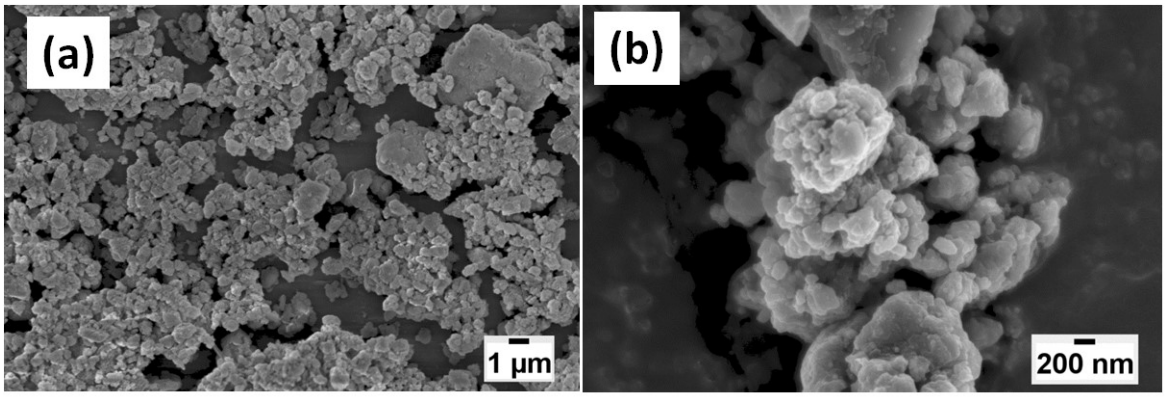

Figure **5.4**. (**a**) and (**b**) are SEM images of Pd(0)/g-C_3N_4O

The surface morphology of the synthesized catalyst is studied by SEM analysis (Figure **5.4**). From the SEM image (Figure **5.4a**), it is observed that the Pd NPs are coated on the surface of the g-C_3N_4O sheet and are uniformly distributed on the surface. Irregular morphology of the catalyst is seen with rough surfaces of the particles.

The bulk morphological study of the catalyst is done by TEM analysis (Figure **5.5**) and the black spots show the distribution of Pd NPs on the graphitic carbon nitride sheet (Figure **5.5a**, **b**). The Pd NPs incorporated on the g-C_3N_4O are almost uniform in size with a diameter in the range of 20-45 nm which is obtained from the particle size distribution histogram (Figure **5.5e**). The HRTEM image of Pd(0)/g-C_3N_4O clearly shows the presence of different crystal planes with lattice spacing of 0.23 and 0.19 nm which corresponds to (111) and (200) crystallographic planes of face-centered cubic (*fcc*) lattice of Pd NPs respectively (Figure **5.5c**). The selected area electron diffraction (SAED) pattern of the catalyst confirms the crystalline nature of the Pd NPs with three

well-resolved rings of the (111), (200), and (220) crystallographic planes of Pd NPs (Figure **5.5d**). The data obtained from TEM analysis agrees well with that of p-XRD analysis.

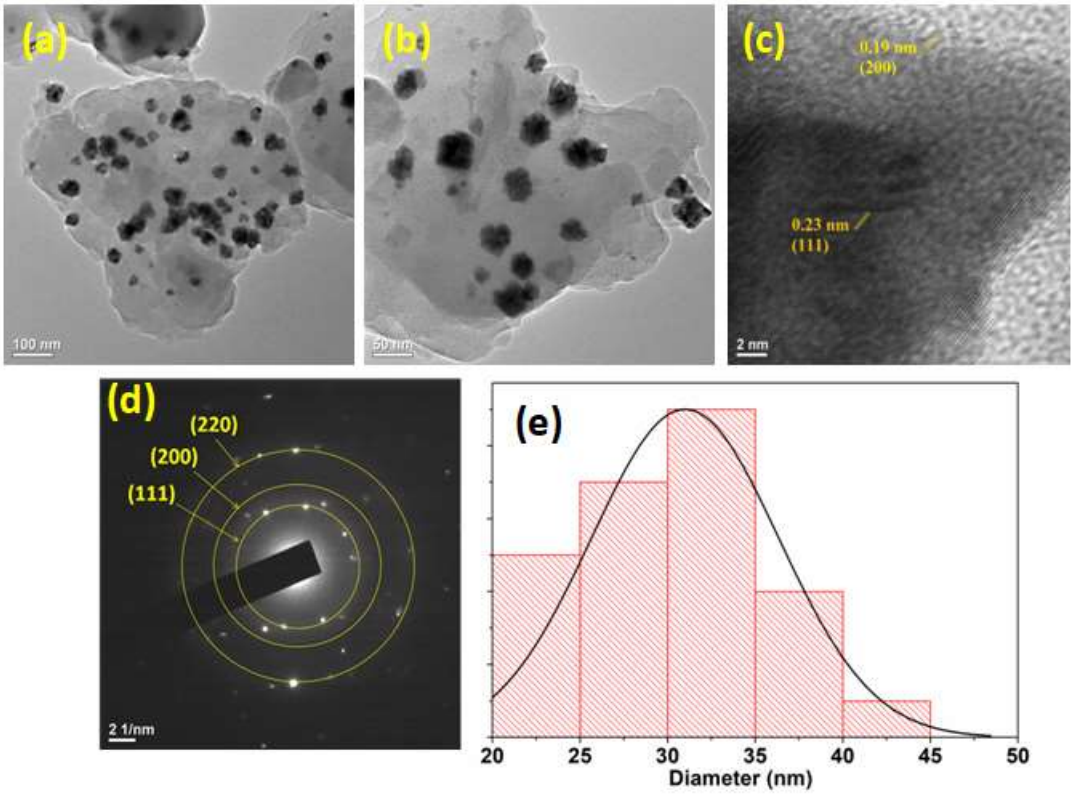

Figure **5.5**. TEM images of (**a**) and (**b**) Pd(0)/g-C_3N_4O, (**c**) HRTEM image, (**d**) SAED pattern, and (**e**) particle size distribution histogram of Pd(0)/g-C_3N_4O.

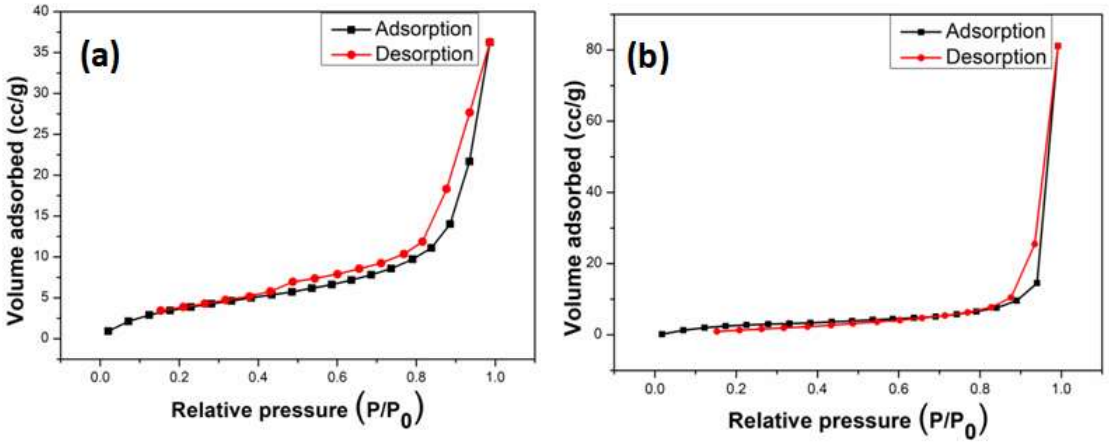

Figure **5.6**. N_2 adsorption/desorption isotherm of (**a**) g-C_3N_4O and (**b**) Pd(0)/g-C_3N_4O

The Brunauer-Emmett-Teller (BET) surface area analysis is done by N_2 adsorption-desorption method at 77 K. The BET isotherms of g-C_3N_4O and Pd(0)/g-C_3N_4O (Figure

5.6a and **5.6b**) are similar to a type IV adsorption isotherm which indicates the mesoporous nature of the adsorbent [26a]. The surface area of g-C_3N_4O and Pd(0)/g-C_3N_4O are found to be 15.93 and 11.84 m^2/g respectively. The pore blockage of mesoporous g-C_3N_4O results in a decrease in surface area after loading of Pd NPs, signifying a strong adsorbate-adsorbent interaction. From the Barrett-Joyner-Halenda (BJH) pore size distribution method, the pore volume and diameter of the synthesized catalyst are found to be 0.130 cc/g and 24.11 nm, respectively.

The elemental composition and the existing bonding information of the Pd in the Pd(0)/g-C_3N_4O nanocomposite is investigated by XPS analysis. The survey spectrum shows the sharp binding energy peak at 285, 399, 336 and 532 eV which are attributed to C, N, Pd and O, respectively (Figure **5.7**). The high resolution spectra of the Pd 3d is deconvoluted with the four binding energy peaks and two spin orbit doublet are assigned to the Pd $3d_{5/2}$ and Pd $3d_{3/2}$ (Figure **5.8a**) The binding energy peak located at 335.8 eV and 341 eV correspond to the Pd(0) NPs and low intensity binding energy peak observed at 336.8 eV and 342 eV are assigned to the Pd(II). This indicates the small amount of the Pd(II) are also present along the Pd(0) on the surface of the g-C_3N_4O. The high resolution C 1s peak deconvoluted to the three peaks 284.6, 285.7 and 288.7 eV are assigned to the C-C/C=C, C=(O, N) and O=C-OH, respectively (Figure **5.8c**). The C=C and C=N bond are due to the sp^2 carbon atom in the *s*-triazine ring in g-C_3N_4O. The high resolution N 1s peak is deconvoluted to two binding energy peaks at 399 and 400.2 eV are assigned to pyridine-like sp^2 (C=N-C) nitrogen of the triazine ring, the nitrogen atom which is trigonally bonded to the carbon atom in the C-N network (N-(C3)), respectively (Figure **5.8b**). The high-resolution O 1s spectrum is deconvoluted with two binding energy peaks at 532.9 and 537.1 eV attributed to the O=C-OH, C-O groups, respectively (Figure **5.8d**).

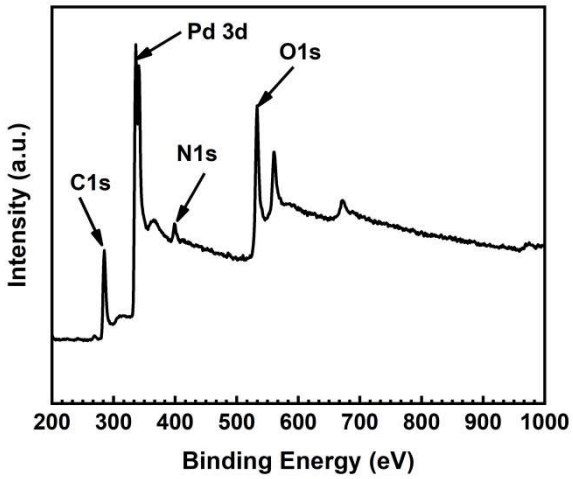

Figure **5.7**. XPS survey spectrum of Pd(0)/g-C_3N_4O

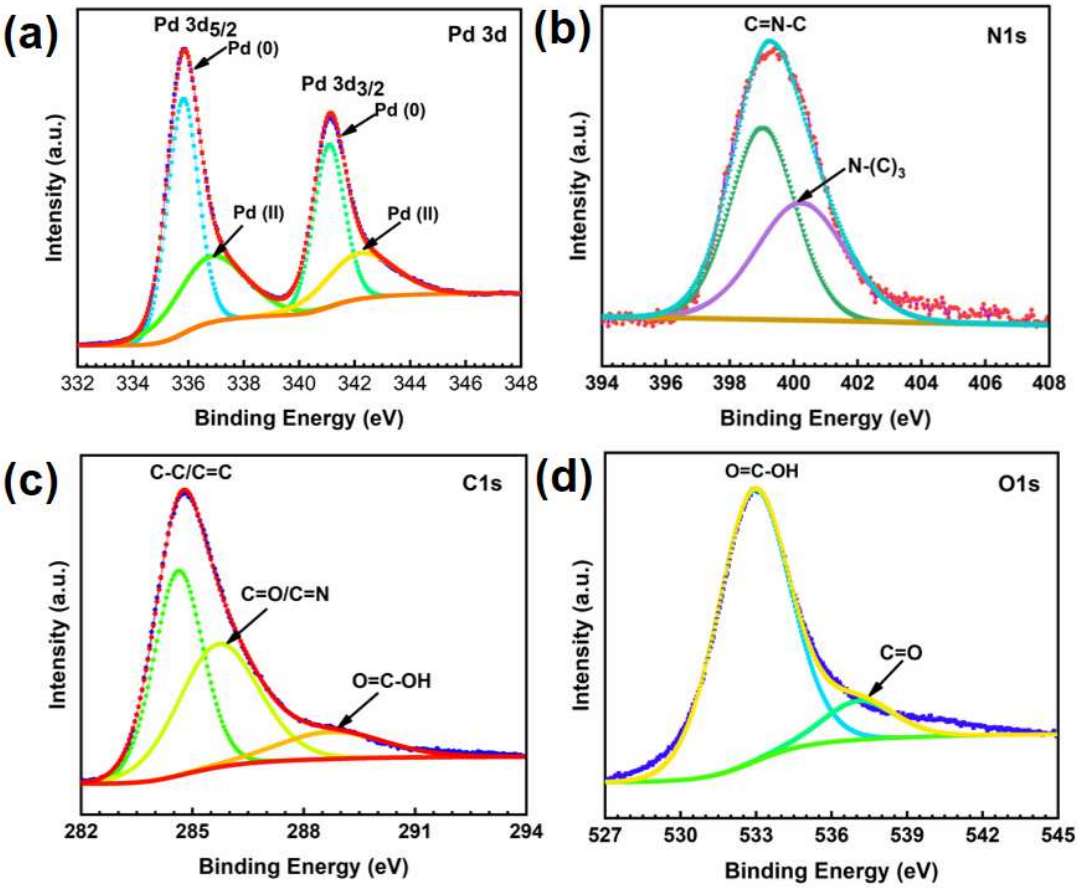

Figure **5.8**. High-resolution deconvoluted XPS spectra of (**a**) Pd 3d; (**b**) N 1s; (**c**) C 1s; (**d**) O 1s of Pd(0)/g-C_3N_4O

5.3.2 Catalytic activity of Pd(0)/g-C_3N_4O

5.3.2.1 Optimization of reaction conditions

To explore the catalytic activity of the synthesized catalyst, we utilized it in Suzuki-Miyaura cross-coupling reaction. The reaction was studied under various reaction conditions and optimization studies were carried out by taking 1-Bromo-4-nitrobenzene and phenylboronic acid as the model substrates. The obtained results are summarized in Table **5.1**.

Table **5.1**. Optimization of amount of substrates, catalyst, base and solvent

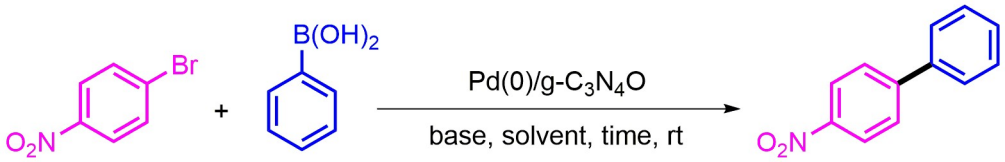

1a **2a** **3a**

Entry	**1a** (equiv.)	**2a** (equiv.)	Pd(0)/g-C_3N_4O (wt%)	Base (equiv.)	Solvent (mL)	Time (h)	Yield[a] (%)
1	1	1.2	10	K_2CO_3 (3)	H_2O	24	25
2	1	1.2	10	K_2CO_3 (3)	EtOH	24	58
3	1	1.2	10	K_2CO_3 (3)	EtOH:H_2O (1:1)	5	98
4	1	1.2	5	K_2CO_3 (3)	EtOH:H_2O (1:1)	5	98
5	1	1.2	5	K_2CO_3 (3)	MeOH: H_2O (1:1)	24	70
6	1	1.2	5	Cs_2CO_3 (3)	EtOH:H_2O (1:1)	5	98
7	1	1.2	2	K_2CO_3 (3)	EtOH:H_2O (1:1)	24	92
8	1	1.2	5	Et_3N (3)	EtOH:H_2O (1:1)	24	48
9	1	1.2	5	K_2CO_3 (2)	EtOH:H_2O (1:1)	5	98
10	1	1.2	5	K_2CO_3 (1)	EtOH:H_2O (1:1)	5	98
11	1	1.2	5	K_2CO_3 (0.5)	EtOH:H_2O (1:1)	5	98
12	1	1.2	5	K_2CO_3 (0.25)	EtOH:H_2O (1:1)	24	40
13	**1**	**1**	**5**	**K_2CO_3 (0.5)**	**EtOH:H_2O (1:1)**	**5**	**98**

[a]Isolated yields

In presence of 10 wt% of the catalyst, the desired product was obtained in 98% yield (entry **3**, Table **5.1**). When we decreased the amount of catalyst to 5 wt%, the yield of the reaction remained the same (entry **4**, Table **5.1**). Further lowering the amount of catalyst to 2 wt% resulted in a decrease in yield (entry **7**, Table **5.1**). Reactions that were carried out only in water or ethanol did not provide very good results, which might be due to the low solubility of substrates in water alone, or poor dispersion of the catalyst in alcoholic medium. Although 98% yield was obtained on the addition of Cs_2CO_3 base also (entry **6**, Table **5.1**), it was preferable to use K_2CO_3 which is a weaker and cheaper base than Cs_2CO_3. A moderate yield of the desired product was attained in presence of Et_3N (entry **8**, Table **5.1**). With 5 wt% of catalyst and EtOH:H_2O (1:1) solvent mixture as the reaction medium, we gradually decreased the amount of K_2CO_3 up to 0.5 equivalent (entry **11**, Table **5.1**) and observed that the yield of the reaction was unchanged (98%). On further decreasing the amount of K_2CO_3 to 0.25 equivalent (entry **12**, Table **5.1**), the yield of the reaction decreased to 40%. Under the base-free conditions, the desired product (10% and 22%) was obtained by performing the reaction at room temperature and 80 °C for 24 hours, respectively. Since the reaction proceeds efficiently with a low amount of base (0.5 equiv.), this indicates that Pd(0)/g-C_3N_4O is a base-functionalized catalyst system. This base-functionalized catalyst activates the boronic acid to such an extent that the addition of a minimum amount of external base (K_2CO_3) is sufficient to carry out the reaction smoothly. The synthesized support g-C_3N_4O is rich in lone pairs of nitrogen and oxygen atoms, which can be easily donated to electrophilic species. The Lewis acidic boronic acid has an affinity towards these lone pairs of electrons to fill its vacant p-orbital. As a result, the activation of boronic acid takes place by forming borate anion which is the most reactive species that enhances the transmetallation of this cross-coupling reaction [26]. Moreover, when we carried out the reaction by using a 1:1 ratio of both substrates, 98% yield (entry **13**, Table **5.1**) of the desired product was obtained.

5.3.2.2 Substrate scope study

With the optimized reaction conditions (entry **13**, Table **5.1**), the scope and limitations of the Suzuki-Miyaura cross-coupling reaction of aryl bromide and boronic acid (and its pinacol ester derivative) were explored and the results are shown in Table **5.2**.

The reaction proceeds efficiently for both electronically and sterically diverse phenylboronic acids and aryl bromides and resulted in good to excellent yields of the

desired product (61-98%). Phenylboronic acids having different functional groups such as –OCH_3 (**3c**, **3j**, **3u**, **3v**, Table **5.2**), −CH_3 (**3d**, **3u**, **3v**, Table **5.2**), −CH_2CH_3 (**3e**, Table **5.2**), −CHO (**3n**, Table **5.2**), −CF_3 (**3l**, Table **5.2**), −F (**3i**, Table **5.2**), −Cl (**3f**, Table **5.2**), $-^tBu$ (**3s**, Table **5.2**), were well-tolerated under the current protocol. Depending upon the position of the substituents (*ortho*, and *meta*), a moderate yield of the desired product was obtained (**3g**, **3h**, **3k**, **3m**, **3o**, **3p**, **3q**, **3r**, Table **5.2**) which might be due to the steric effect of the substituents. We have also carried out the reaction for heteroaryl bromides. The reaction between 3-bromopyridine and phenylboronic acid gave only 17% yield of the desired product at room temperature even after 24 hours. On increasing the temperature up to 60 °C, the reaction resulted in 51% yield. On further increasing the temperature to 80 °C, the reaction furnished 82% yield of the desired product after 5 hours (**3w**, Table **5.2**). Similarly, 5-bromopyrimidine on reaction with phenylboronic acid resulted in 74% yield of the desired product (**3x**, Table **5.2**). Interestingly, Phenylboronic acid pinacol ester also showed excellent reactivity under the developed reaction condition and furnished good yields of the desired product (**3y**, **3z**, Table **5.2**). The TON and TOF values of the catalyst were found to be 649.13 and 129.83 h^{-1} respectively.

Table **5.2**. Substrate scope for Pd(0)/g-C_3N_4O catalyzed Suzuki coupling[a]

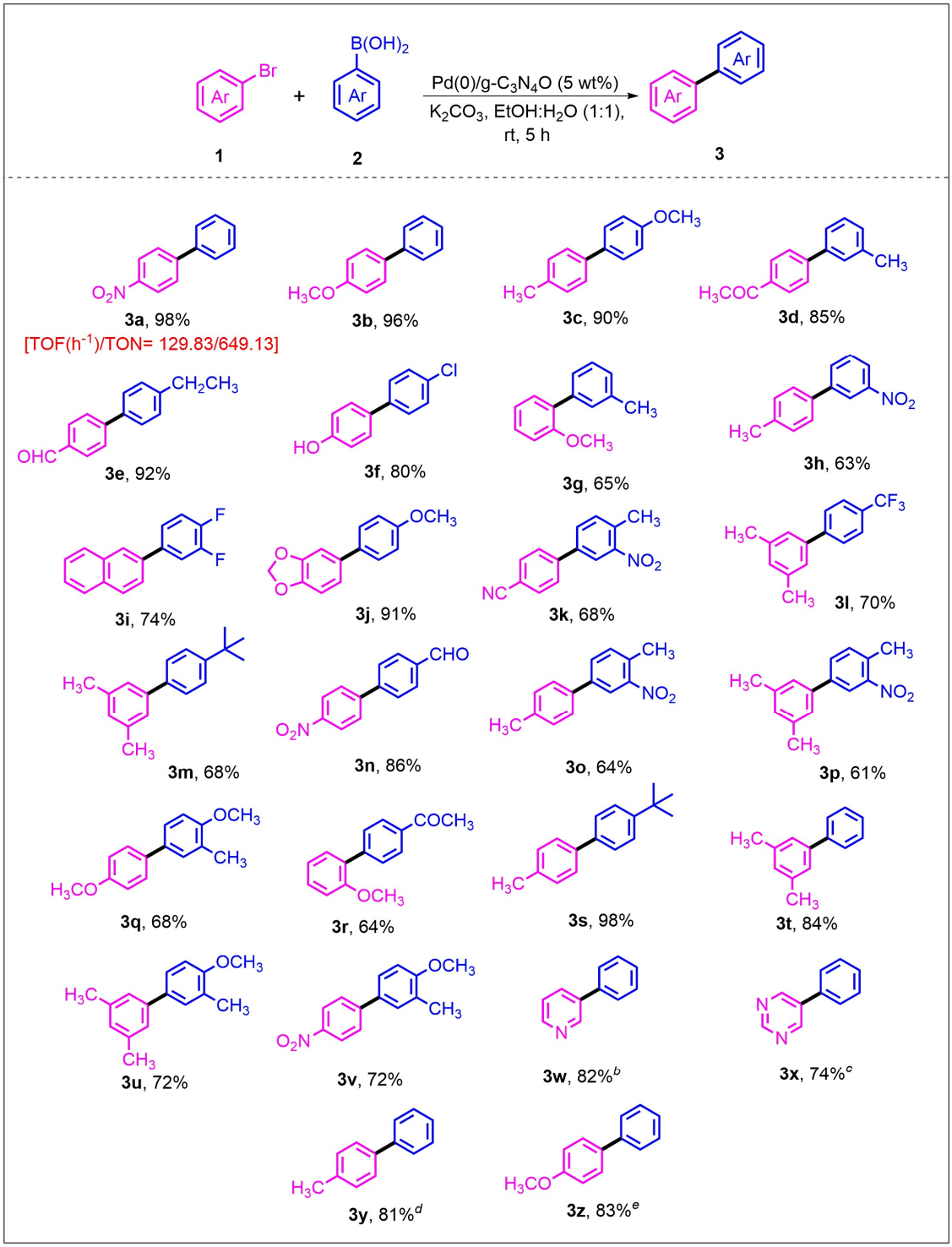

[a]Reaction conditions: **1** (1 equiv.), **2** (1 equiv.), K_2CO_3 (0.5 equiv.), EtOH:H_2O (4 mL), [b, c]Reactions were carried out at 80 °C. [d, e]Phenylboronic acid pinacol ester was used as the boronic acid counterpart. TON (Turnover number: Yield of product/per mol of Pd), TOF (Turnover frequency: TON/reaction time)

5.3.2.3 Heterogeneity test

To confirm the heterogeneous nature of the catalyst, initially, the reaction was carried out by adding Pd(0)/g-C_3N_4O (5 wt%), and K_2CO_3 (0.25 mmol) in EtOH:H_2O (1:1) mixture at room temperature for 2.5 hours without using the substrates. Then the reaction mixture was filtered and to that filtrate 1-Bromo-4-nitrobenzene and phenylboronic acid were added and stirred for 5 hours at room temperature. A trace amount of product formation was observed which indicated the heterogeneous nature of the catalyst. Further, the ICP-OES analysis of the liquid phase revealed that the concentration of residual Pd is less than 1 ppm.

5.3.2.4 Reusability test

Reusability is an important aspect of the catalyst from green chemistry as well as the commercial point of view. In our protocol, the synthesized catalyst was recycled for five cycles (Figure **5.9**). There were slight changes in the reactivity of the catalyst over the consecutive cycles which might be due to the physical loss of the catalyst. For the recyclability test, the used catalyst was recovered by centrifugation from the reaction mixture, washed with ethyl acetate, ethanol and water. After that, the recovered catalyst was dried in a vacuum desiccator and used in the next cycle.

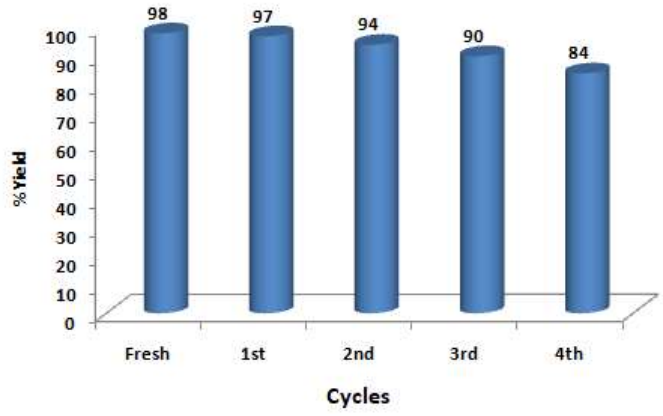

Figure **5.9**. Reusability test of Pd(0)/g-C_3N_4O

The TEM images (Figure **5.10a**, **b**) of the reused catalyst after the fifth cycle show the distribution of Pd NPs on the graphitic carbon nitride sheet. HRTEM image confirmed the presence of a crystal plane (200) with a lattice spacing 0.20 nm (Figure **5.10c**). Moreover, SAED pattern of the reused catalyst is similar to that of the fresh catalyst with

three well-resolved rings that correspond to (111), (200), and (220) crystallographic planes of Pd NPs (Figure **5.10d**).

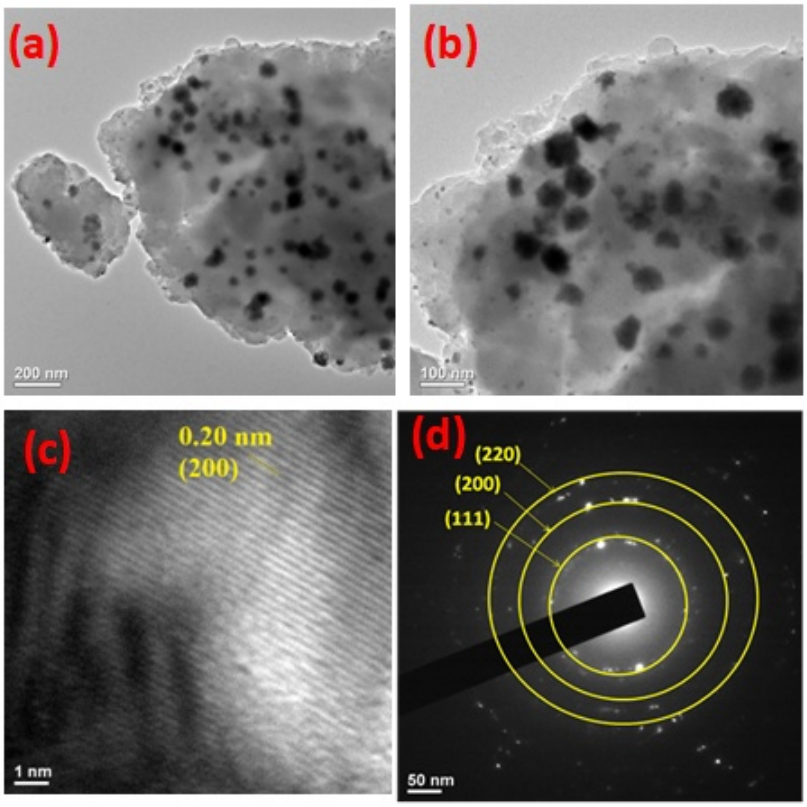

Figure **5.10**. (**a**) and (**b**) TEM images of reused catalyst, (**c**) HRTEM and (**d**) SAED pattern

5.3.2.5 Control experiment

To understand the role of Pd(0)/g-C_3N_4O as a heterogeneous catalyst, we carried out control experiments and the results obtained are summarized in Table **5.3**. The formation of biaryl was not observed with the separate addition of $Pd(OAc)_2$ (0.008 mmol, amount of Pd as per in the developed catalyst) and g-C_3N_4O sheet (entry **1**, Table **5.3**). Addition of K_2CO_3 (0.5 equiv.) along with $Pd(OAc)_2$/g-C_3N_4O and $Pd(OAc)_2$/Pomegranate extract, did not furnish satisfactory results (entries **2** and **3**, Table **5.3**). A low yield (27%) of the desired product was obtained under homogeneous reaction conditions [$Pd(OAc)_2$, Pomegranate extract, g-C_3N_4O, K_2CO_3 (0.5 equiv.)] (entry **4**, Table **5.3**). The control experiments indicated that the pre-synthesis of Pd(0)/g-C_3N_4O using pomegranate peel extract was essential to get an active catalytic system.

Table **5.3**. Control experiments

Entry	Reaction conditions	Result
1	$Pd(OAc)_2$/g-C_3N_4O	NR
2	$Pd(OAc)_2$/g-C_3N_4O/K_2CO_3 (0.5 equiv.)	Trace
3	$Pd(OAc)_2$/Pomegranate extract/K_2CO_3 (0.5 equiv.)	Trace
4	$Pd(OAc)_2$/Pomegranate extract/g-C_3N_4O/K_2CO_3 (0.5 equiv.)	27%

5.3.2.6 Plausible Mechanism

Accordingly, the plausible mechanism (Scheme **5.11**) of the S−M reaction is proposed. The nitrogen functionalities of the g-C_3N_4O sheet act as anchoring sites for homogeneous dispersion and stabilization of Pd NPs. The π−π stacking interaction between aryl halides and the g-C_3N_4O sheet enhanced the reaction as the aryl halides could easily get access to Pd NPs on the g-C_3N_4O surface. The mechanism then involves the three steps of an organometallic cycle: oxidative addition of the aryl halide to Pd(0)/g-C_3N_4O to form the corresponding Pd(II) species (**A**); activation of boronic acid by the exogenous base (K_2CO_3) along with lone pairs of nitrogen and oxygen atoms to form the boronate species (**B**) and facilitate transmetallation; and finally reductive elimination to furnish the desired biaryl derivative (**C**). Thus, the developed heterogeneous catalyst system can effectively provide biaryls in good to excellent yields by minimizing the base stoichiometry.

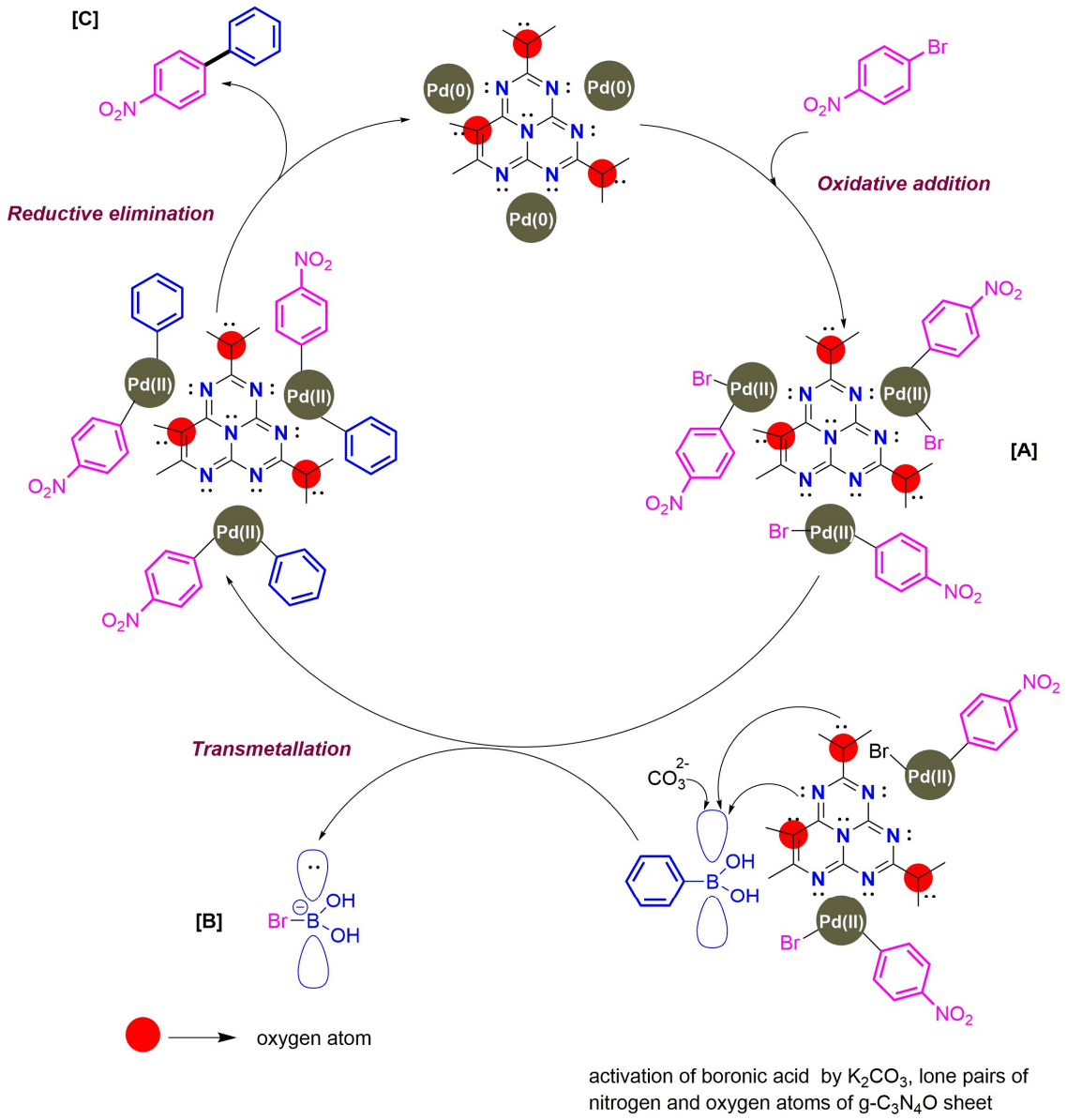

Scheme **5.11**. Proposed mechanism of Suzuki-Miyaura cross-coupling with Pd(0)/g-C_3N_4O.

5.4 Conclusion

In summary, we have developed a heterogeneous catalytic system through the immobilization of Pd NPs on g-C_3N_4O sheet and applied the synthesized catalyst for Suzuki-Miyaura cross-coupling reaction. Unlike previously reported works, the developed catalyst system could successfully facilitate the reaction in presence of a minimum amount of exogenous base (0.5 equiv.) and with an equimolar amount of both the substrates in good to excellent yields of the desired products. The methodology was suitable for substrates having different electronic and steric environments under mild

reaction conditions. This bio-based catalyst could be reused for up to five consecutive reaction cycles and its true heterogeneity was confirmed by experimental results. The high efficiency of the developed catalyst [Pd(0)/g-C_3N_4O] in Suzuki-Miyaura cross-coupling reaction at room temperature in an aqueous medium under an air atmosphere, achieves the demand for a sustainable catalytic process.

5.5 ^{1}H and ^{13}C NMR analytical data

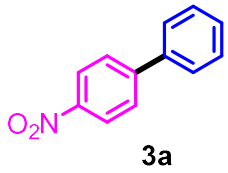

3a

4-nitro-1,1'-biphenyl (3a): ^{1}H NMR (400 MHz, $CDCl_3$): δ (ppm) 8.30–8.24 (m, 2H), 7.75–7.68 (m, 2H), 7.63–7.59 (m, 2H), 7.52–7.41 (m, 3H); ^{13}C NMR (100 MHz, $CDCl_3$): δ (ppm) 147.7, 147.2, 138.8, 129.3, 127.9, 127.6, 127.5, 124.6.

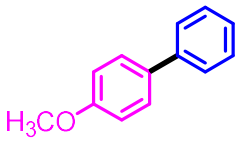

3b

4-methoxy-1,1'-biphenyl (3b): ^{1}H NMR (400 MHz, $CDCl_3$): δ (ppm) 7.58–7.49 (m, 4H), 7.46–7.37 (m, 2H), 7.36–7.26 (m, 1H), 7.01–6.94 (m, 2H), 3.85 (s, 3H); ^{13}C NMR (100 MHz, $CDCl_3$): δ (ppm) 159.2, 141.1, 134.1, 128.9, 128.3, 126.9, 126.7, 114.7, 55.4.

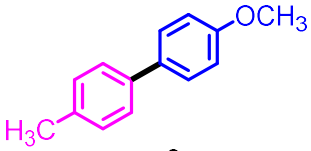

3c

4-methoxy-4'-methyl-1,1'-biphenyl (3c): ^{1}H NMR (400 MHz, $CDCl_3$): δ (ppm) 7.54–7.41 (m, 4H), 7.22 (dd, J = 8.4, 0.6 Hz, 2H), 6.99–6.93 (m, 2H), 3.84 (s, 3H), 2.38 (s, 3H); ^{13}C NMR (100 MHz, $CDCl_3$): δ (ppm) 159.2, 138.0, 136.7, 134.1, 130.2, 128.4, 127.0, 114.7, 55.8, 21.5.

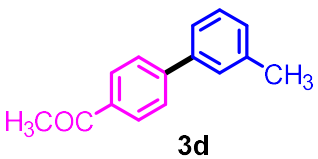

3d

1-(3'-methyl-[1,1'-biphenyl]-4-yl)ethan-1-one (3d): ^{1}H NMR (400 MHz, $CDCl_3$): δ (ppm) 8.04–7.99 (m, 2H), 7.70–7.64 (m, 2H), 7.41 (dd, J = 4.6, 4.1 Hz, 2H), 7.35 (t, J = 7.5 Hz, 1H), 7.21 (dd, J = 4.3, 3.7 Hz, 1H), 2.62 (dd, J = 2.6, 0.5 Hz, 3H), 2.43 (s, 3H); ^{13}C NMR (100 MHz, $CDCl_3$): δ (ppm) 198.3, 146.1, 140.0, 138.7, 135.8, 129.0, 128.2, 128.1, 127.4, 124.5, 124.4, 26.7, 21.9

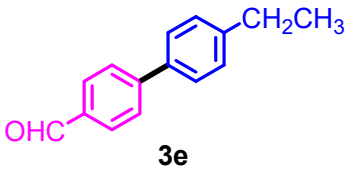

3e

4'-ethyl-[1,1'-biphenyl]-4-carbaldehyde (3e): ^{1}H NMR (400 MHz, $CDCl_3$): δ (ppm) 10.03 (s, 1H), 7.95–7.90 (m, 2H), 7.76–7.71 (m, 2H), 7.60–7.53 (m, 2H), 7.34–7.28 (m, 2H), 2.80–2.61 (m, 2H), 1.31–1.21 (m, 3H); ^{13}C NMR (100 MHz, $CDCl_3$): δ (ppm) 192.1, 147.3, 145.0, 137.1, 135.1, 130.4, 128.6, 127.5, 127.4, 28.6, 15.8.

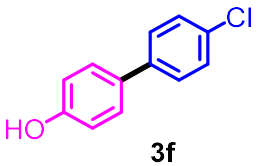

3f

4'-chloro-[1,1'-biphenyl]-4-ol (3f): ^{1}H NMR (400 MHz, $CDCl_3$): δ (ppm) 7.49–7.32 (m, 6H), 6.93–6.86 (m, 2H), 4.94 (s, 1H); ^{13}C NMR (100 MHz, $CDCl_3$): δ (ppm) 155.2, 139.4, 132.9, 132.8, 129.0, 128.4, 128.1, 116.0.

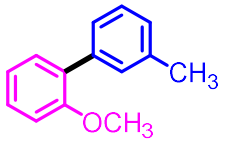

3g

2-methoxy-3'-methyl-1,1'-biphenyl (3g): ^{1}H NMR (400 MHz, $CDCl_3$): δ (ppm) 7.44–7.33 (m, 5H), 7.24–7.18 (m, 1H), 7.11–7.01 (m, 2H), 3.85 (d, J = 1.3 Hz, 3H), 2.46 (s, 3H); ^{13}C NMR (100 MHz, $CDCl_3$): δ (ppm) 156.7, 138.7, 137.7, 131.0, 130.4, 130.3, 128.8, 128.0, 120.9, 111.2, 56.3, 21.9.

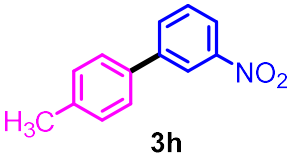

3h

4'-methyl-3-nitro-1,1'-biphenyl (3h): ^{1}H NMR (400 MHz, $CDCl_3$): δ (ppm) 8.44–8.41 (m, 1H), 8.18–8.14 (m, 1H), 7.91–7.86 (m, 1H), 7.61–7.49 (m, 3H), 7.31–7.27 (m, 2H), 2.41 (s, 3H); ^{13}C NMR (100 MHz, $CDCl_3$): δ (ppm) 148.8, 142.9, 138.7, 135.8, 133.0, 130.0, 129.9, 129.7, 127.1, 121.8, 21.3.

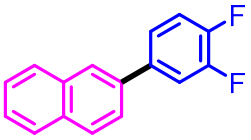

3i

2-(3,4-difluorophenyl)naphthalene (3i): ^{1}H NMR (400 MHz, $CDCl_3$): δ (ppm) 7.96 (s, 1H), 7.93–7.80 (m, 3H), 7.64 (dd, J = 8.5, 1.7 Hz, 1H), 7.56–7.38 (m, 4H), 7.31–7.18 (m, 1H); ^{13}C NMR (100 MHz, $CDCl_3$): δ (ppm) 151.5, 149.5, 138.4, 136.6, 132.8, 128.8, 128.4, 127.9, 126.7, 126.4, 125.9, 125.1, 123.4.

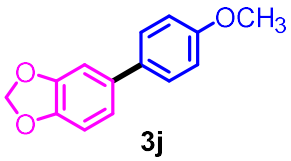

3j

5-(4-methoxyphenyl)benzo[1,3]dioxole (3j): ^{1}H NMR (400 MHz, $CDCl_3$): δ (ppm) 7.48–7.39 (m, 2H), 7.04–6.91 (m, 4H), 6.88–6.82 (m, 1H), 6.01–5.94 (m, 2H), 3.83 (s, 3H); ^{13}C NMR (100 MHz, $CDCl_3$): δ (ppm) 159.0, 148.2, 146.7, 135.4, 133.8, 127.9, 120.3, 114.3, 108.7, 107.5, 101.1, 55.8.

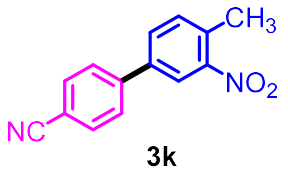

3k

4'-methyl-3'-nitro-[1,1'-biphenyl]-4-carbonitrile (3k): ^{1}H NMR (600 MHz, $CDCl_3$): δ (ppm) 7.92–7.83 (m, 1H), 7.48–7.32 (m, 5H), 7.13 (dd, J = 9.6, 5.3 Hz, 1H), 6.98–6.86 (m, 1H), 2.43–2.28 (m, 3H); ^{13}C NMR (150 MHz, $CDCl_3$): δ (ppm) 149.4, 142.6, 137.9, 133.6, 133.4, 132.6, 131.0, 127.3, 122.9, 118.2, 111.7, 19.9.

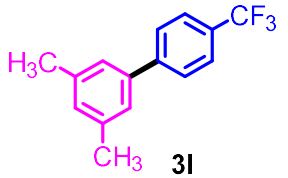

3l

3,5-dimethyl-4'-(trifluoromethyl)-1,1'-biphenyl (3l): ^{1}H NMR (400 MHz, $CDCl_3$): δ (ppm) 7.66 (s, 4H), 7.20 (s, 2H), 7.05 (d, J = 0.5 Hz, 1H), 2.42–2.36 (m, 6H); ^{13}C NMR (100 MHz, $CDCl_3$): δ (ppm) 145.1, 139.9, 138.7, 129.4, 127.5, 125.7, 125.2, 123.2, 21.7.

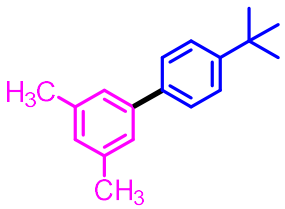

3m

4'-(*tert*-butyl)-3,5-dimethyl-1,1'-biphenyl (3m): ^{1}H NMR (500 MHz, $CDCl_3$): δ (ppm) 7.63–7.59 (m, 2H), 7.55–7.52 (m, 2H), 7.29 (d, J = 6.8 Hz, 2H), 7.06 (s, 1H), 2.46 (s, 6H), 1.45 (s, 9H); ^{13}C NMR (125 MHz, $CDCl_3$): δ (ppm) 150.0, 141.1, 138.1, 128.6, 126.8, 126.6, 125.5, 124.9, 34.4, 31.3, 21.4.

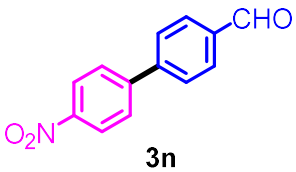

3n

4'-nitro-[1,1'-biphenyl]-4-carbaldehyde (3n): ^{1}H NMR (500 MHz, $CDCl_3$): δ (ppm) 10.11 (s, 1H), 8.35 (d, J = 8.9 Hz, 2H), 8.03 (d, J = 8.4 Hz, 2H), 7.83–7.77 (m, 4H); ^{13}C NMR (125 MHz, $CDCl_3$): δ (ppm) 191.5, 147.7, 145.9, 144.4, 136.2, 130.3, 128.1, 128.0, 124.2.

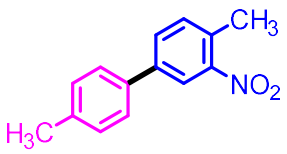

3o

4,4'-dimethyl-3-nitro-1,1'-biphenyl (3o): ^{1}H NMR (500 MHz, $CDCl_3$): δ (ppm) 8.21 (d, J = 1.9 Hz, 1H), 7.73 (dd, J = 7.9, 1.9 Hz, 1H), 7.54–7.49 (m, 2H), 7.39 (dd, J = 11.7, 4.6 Hz, 1H), 7.30 (dd, J = 10.8, 3.0 Hz, 2H), 2.65 (s, 3H), 2.44 (s, 3H); ^{13}C NMR (125 MHz, $CDCl_3$): δ (ppm) 149.5, 140.1, 138.1, 135.5, 133.1, 131.8, 131.0, 129.7, 126.6, 122.6, 21.0, 20.0.

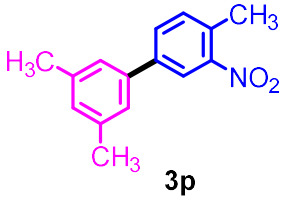

3p

3',4,5'-trimethyl-3-nitro-1,1'-biphenyl (3p): ^{1}H NMR (500 MHz, $CDCl_3$): δ (ppm) 8.22 (d, J = 1.9 Hz, 1H), 7.73 (dd, J = 7.9, 2.0 Hz, 1H), 7.40 (d, J = 8.0 Hz, 1H), 7.24 (s, 2H), 7.08–7.05 (m, 1H), 2.66 (s, 3H), 2.42 (s, 6H); ^{13}C NMR (125 MHz, $CDCl_3$): δ (ppm) 149.4, 140.5, 138.6, 138.4, 133.0, 131.9, 131.2, 129.8, 124.7, 122.8, 21.3, 20.0.

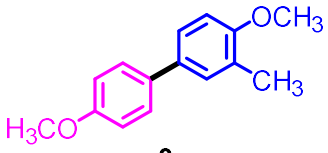

3q

4,4'-dimethoxy-3-methyl-1,1'-biphenyl (3q): ^{1}H NMR (500 MHz, $CDCl_3$): δ (ppm) 7.55–7.48 (m, 2H), 7.38 (dd, J = 6.0, 2.2 Hz, 2H), 7.02–6.97 (m, 2H), 6.94–6.88 (m, 1H), 3.90 (s, 3H), 3.88 (s, 3H), 2.32 (s, 3H); ^{13}C NMR (125 MHz, $CDCl_3$): δ (ppm) 158.5, 156.8, 133.6, 133.0, 129.1, 127.6, 126.7, 124.8, 114.0, 110.1, 55.3, 55.2, 16.3.

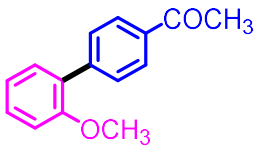

3r

1-(2'-methoxy-[1,1'-biphenyl]-4-yl)ethan-1-one (3r): ^{1}H NMR (500 MHz, $CDCl_3$): δ (ppm) 8.08–7.99 (m, 2H), 7.73–7.62 (m, 2H), 7.46–7.34 (m, 2H), 7.15–6.98 (m, 2H), 3.85 (s, 3H), 2.66 (s, 3H); ^{13}C NMR (125 MHz, $CDCl_3$): δ (ppm) 197.8, 156.4, 143.5, 135.4, 130.6, 129.6, 129.4, 129.3, 128.0, 120.9, 111.3, 55.5, 26.5.

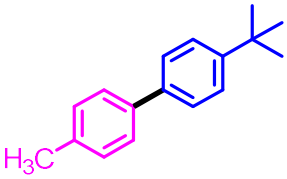

3s

4-(*tert*-butyl)-4'-methyl-1,1'-biphenyl (3s): ^{1}H NMR (500 MHz, $CDCl_3$): δ (ppm) 7.60–7.49 (m, 6H), 7.31–7.26 (m, 2H), 2.44 (s, 3H), 1.42 (s, 9H); ^{13}C NMR (125 MHz, $CDCl_3$): δ (ppm) 149.8, 138.2, 136.6, 129.3, 126.8, 126.5,

125.6, 125.5, 34.4, 31.3, 21.0.

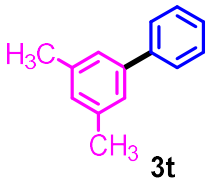

3t

3,5-dimethyl-1,1'-biphenyl (3t): ^{1}H NMR (500 MHz, $CDCl_3$): δ (ppm) 7.73 (d, J = 7.1 Hz, 2H), 7.60–7.46 (m, 4H), 7.37 (s, 2H), 7.14 (s, 1H), 2.53 (s, 6H); ^{13}C NMR (125 MHz, $CDCl_3$): δ (ppm) 141.5, 141.3, 138.2, 128.9, 128.7, 127.2, 127.1, 125.1, 21.4.

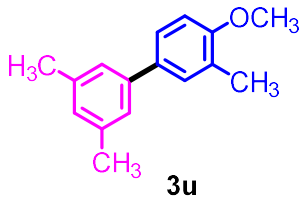

3u

4-methoxy-3,3',5'-trimethyl-1,1'-biphenyl (3u): ^{1}H NMR (500 MHz, $CDCl_3$): δ (ppm) 7.49–7.46 (m, 3H), 7.28 (s, 1H), 7.05–6.95 (m, 2H), 3.94 (s, 3H), 2.47 (s, 6H), 2.39(s, 3H); ^{13}C NMR (125 MHz, $CDCl_3$): δ (ppm) 157.2, 138.1, 133.5, 129.5, 129.0, 128.2, 126.7, 125.3, 124.7, 110.0, 55.3, 21.4, 16.3.

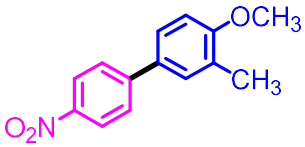

3v

4-methoxy-3-methyl-4'-nitro-1,1'-biphenyl (3v): ^{1}H NMR (500 MHz, $CDCl_3$): δ (ppm) 8.31–8.24 (m, 2H), 7.74–7.68 (m, 2H), 7.46 (d, J = 5.9 Hz, 2H), 6.95 (d, J = 8.4 Hz, 1H), 3.92 (s, 3H), 2.32 (s, 3H); ^{13}C NMR (125 MHz, $CDCl_3$): δ (ppm) 158.6, 147.4, 146.3, 130.5, 129.5, 127.4, 126.9, 125.8, 124.0, 110.2, 55.4, 16.3.

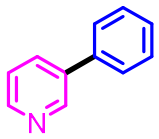

3w

3-phenylpyridine (3w): ^{1}H NMR (400 MHz, $CDCl_3$): δ (ppm) 8.87–8.80 (m, 1H), 8.60–8.53 (m, 1H), 7.89–7.82 (m, 1H), 7.59–7.53 (m, 2H), 7.49–7.30 (m, 4H); ^{13}C NMR (125 MHz, $CDCl_3$): δ (ppm) 148.5, 148.4, 137.9, 136.8, 134.5, 129.3, 128.2, 127.2, 123.8.

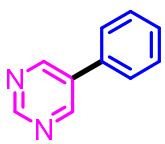

3x

5-phenylpyrimidine (3x): ^{1}H NMR (400 MHz, $CDCl_3$): δ (ppm) 9.20–9.16 (m, 1H), 8.93 (d, J = 3.3 Hz, 2H), 7.58–7.54 (m, 2H), 7.52–7.42 (m, 3H); ^{13}C NMR (125 MHz, $CDCl_3$): δ (ppm) 157.6, 157.5, 155.0, 134.4, 134.3, 129.6, 129.1, 127.1.

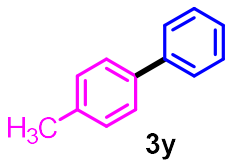

3y

4-methyl-1,1'-biphenyl (3y): ^{1}H NMR (500 MHz, $CDCl_3$): δ (ppm) 7.66–7.61 (m, 2H), 7.55 (d, J = 8.1 Hz, 2H), 7.48 (dd, J = 10.6, 4.8 Hz, 2H), 7.40–7.35 (m, 1H), 7.32–7.28 (m, 2H), 2.45 (s, 3H); ^{13}C NMR (125 MHz, $CDCl_3$): δ (ppm) 141.1, 138.3, 136.9, 129.4, 128.6, 126.9, 126.8, 21.0.

^{1}H and ^{13}C NMR spectra of 4,4'-dimethyl-3-nitro-1,1'-biphenyl

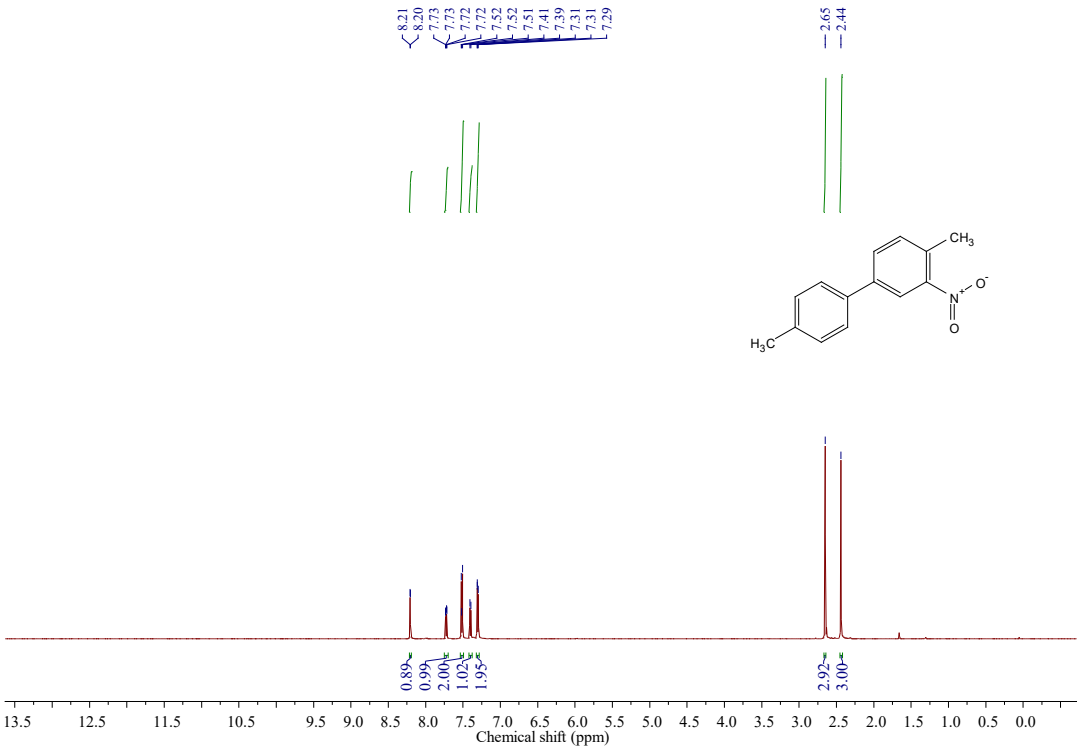

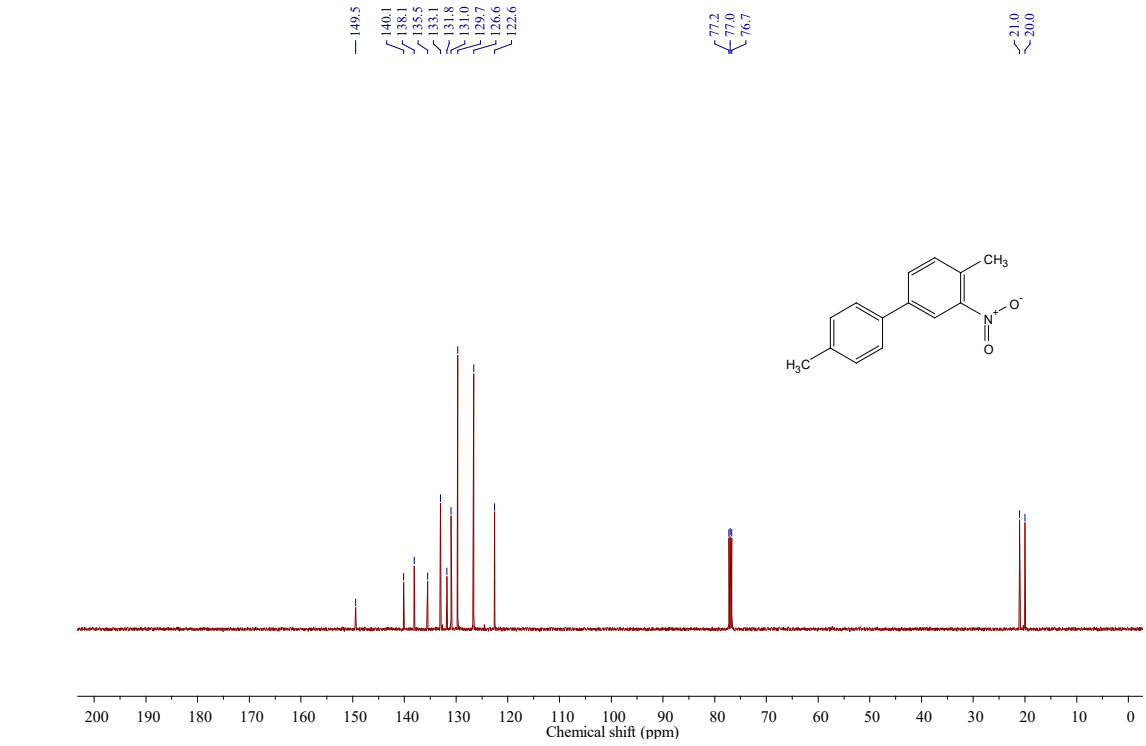

5.6 Bibliography

[1] Delaney, C. P., Marron, D. P., Shved, A. S., Zare, R. N., Waymouth, R. M., and Denmark, S. E. Potassium Trimethylsilanolate-Promoted, Anhydrous Suzuki–Miyaura Cross-Coupling Reaction Proceeds *via* the "Boronate Mechanism": Evidence for the Alternative Fork in the Trail. *Journal of the American Chemical Society*, 144(10):4345-4364, 2022. (b) Kandathil, V., Kulkarni, B., Siddiqa, A., Kempasiddaiah, M., Sasidhar, B. S., Patil, S. A., and Patil, S. A. Immobilized N-Heterocyclic Carbene-Palladium(II) Complex on Graphene Oxide as Efficient and Recyclable Catalyst for Suzuki–Miyaura Cross-Coupling and Reduction of Nitroarenes. *Catalysis Letters*, 150(2):384-403, 2020. (c) Mondal, M. and Bora, U. An efficient protocol for palladium-catalyzed ligand-free Suzuki–Miyaura coupling in water. *Green Chemistry*, 14(7):1873-1876, 2012.

[2] (a) Lima, C. F., Rodrigues, A. S., Silva, V. L., Silva, A. M., and Santos, L. M. Role of the Base and Control of Selectivity in the Suzuki–Miyaura Cross-Coupling Reaction. *ChemCatChem*, 6(5):1291-1302, 2014. (b) Carrow, B. P. and Hartwig, J. F. Distinguishing between pathways for transmetallation in Suzuki−Miyaura reactions. *Journal of the American Chemical Society*, 133(7):2116-2119, 2011.

[3] Bhardwaj, M., Sahi, S., Mahajan, H., Paul, S., and Clark, J. H. Novel heterogeneous catalyst systems based on Pd(0) nanoparticles onto amine functionalized silica-cellulose substrates [Pd (0)-EDA/SCs]: synthesis, characterization and catalytic activity toward C–C and C–S coupling reactions in water under limiting basic conditions. *Journal of Molecular Catalysis A: Chemical*, 408:48-59, 2015.

[4] (a) D'Alterio, M. C., Casals-Cruañas, È., Tzouras, N. V., Talarico, G., Nolan, S. P., and Poater, A. Mechanistic Aspects of the Palladium-Catalyzed Suzuki-Miyaura Cross-Coupling Reaction. *Chemistry–A European Journal*, 27(54):13481-13493, 2021. (b) Kalay, E. Investigation of the activity of palladium nanoparticles supported on mesoporous graphitic carbon nitride in Heck and Suzuki cross-coupling reactions. *Synthetic Communications*, 52(9-10):1290-1305, 2022.

[5] (a) Sharma, R. K., Dutta, S., Sharma, S., Zboril, R., Varma, R. S., and Gawande, M. B. Fe_3O_4 (iron oxide)-supported nanocatalysts: synthesis, characterization and applications in coupling reactions. *Green Chemistry*, 18(11):3184-3209, 2016. (b) Rivallan, M., Thomas, S., Lepage, M., Takagi, N., Hirata, H., and Thibault-Starzyk, F. Evolution of platinum particles dispersed on zeolite upon oxidation catalysis and ageing. *ChemCatChem*, 2(12):1599-1605, 2010. (c) Bansal, V. K., Thankachan, P. P., and Prasad, R. Oxidation of benzyl alcohol and styrene using H_2O_2 catalyzed by tetraazamacrocycle complexes of Cu(II) and Ni(II) encapsulated in zeolite-Y. *Applied Catalysis A: General*, 381(1-2):8-17, 2010. (d) Baran, T., Sargin, I., Kaya, M., Menteş, A., and Ceter, T. Design and application of sporopollenin microcapsule supported palladium catalyst: Remarkably high turnover frequency and reusability in catalysis of biaryls. *Journal of Colloid and Interface Science*, 486:194-203, 2017.

[6] (a) Mart, M., Tylus, W., and Trzeciak, A. M. Pd/DNA as highly active and recyclable catalyst of Suzuki–Miyaura coupling. *Catalysts*, 8(11):552, 2018. (b) Neshat, A., Gholinejad, M., Özcan, H., Khosravi, F., Mobarakeh, A. M., and Zaim, Ö. Suzuki coupling reactions catalyzed by Schiff base supported palladium complexes bearing the vitamin B6 cofactor. *Molecular Catalysis*, 505:111528, 2021.

[7] (a) Das, S. K., Dewan, A., Deka, P., Saikia, R., Thakuria, S., Deka, R. C., Thakur, A. J., and Bora, U. Biogenic palladium nanostructures for Suzuki-Miyaura and Sonogashira cross-coupling reaction under mild reaction conditions. *Current Research in Green and Sustainable Chemistry*, 5:100301, 2022. (b) Şahin Ün, Ş., Ünlü, A., Ün, İ., and Ok, S. Green synthesis, characterization and catalytic activity evaluation of palladium nanoparticles facilitated by Punica granatum peel extract. *Inorganic and Nano-Metal Chemistry*, 51(9):1232-1240, 2021. (c) Sivamaruthi, B. S., Ramkumar, V. S., Archunan, G., Chaiyasut, C., and Suganthy, N. Biogenic synthesis of silver palladium bimetallic nanoparticles from fruit extract of Terminalia chebula-In vitro evaluation of anticancer and antimicrobial activity. *Journal of Drug Delivery Science and Technology*, 51:139-151, 2019. (d) Borah, R. K., Mahanta, A., Dutta, A., Bora, U., and Thakur, A. J. A green synthesis of palladium nanoparticles by Sapindus

mukorossi seed extract and use in efficient room temperature Suzuki–Miyaura cross-coupling reaction. *Applied Organometallic Chemistry*, 31(11):3784, 2017. (e) Yates, M. D., Cusick, R. D., and Logan, B. E. Extracellular palladium nanoparticle production using Geobacter sulfurreducens. *ACS Sustainable Chemistry & Engineering*, 1(9):1165-1171, 2013.

[8] (a) Liu, Q. and Zhang, J. Graphene supported Co-g-C_3N_4 as a novel metal–macrocyclic electrocatalyst for the oxygen reduction reaction in fuel cells. *Langmuir*, 29(11):3821-3828, 2013. (b) Kumar, Y., Rani, S., Shabir, J., and Kumar, L. S. Nitrogen-rich and porous graphitic carbon nitride nanosheet-immobilized palladium nanoparticles as highly active and recyclable catalysts for the reduction of nitro compounds and degradation of organic dyes. *ACS Omega*, 5(22):13250-13258, 2020. (c) Zhang, Y., Liu, J., Wu, G., and Chen, W. Porous graphitic carbon nitride synthesized *via* direct polymerization of urea for efficient sunlight-driven photocatalytic hydrogen production. *Nanoscale*, 4(17):5300-5303, 2012.

[9] (a) Long, X., Chen, W., Lei, C., Xie, Q., Zhang, F., and Huang, B. Ultrafine Pd nanoparticles @ g-C_3N_4 for highly efficient dehalogenation of chlorinated environmental pollutant: Structure, efficacy and mechanisms. *Science of the Total Environment*, 775:145178, 2021. (b) Ma, J., Yang, Q., Wen, Y., and Liu, W. Fe-g-C_3N_4/graphitized mesoporous carbon composite as an effective Fenton-like catalyst in a wide pH range. *Applied Catalysis B: Environmental*, 201:232-240, 2017.

[10] (a) Cao, S., Low, J., Yu, J., and Jaroniec, M. Polymeric photocatalysts based on graphitic carbon nitride. *Advanced Materials*, 27(13):2150-2176, 2015. (b) Ajiboye, T. O., Kuvarega, A. T., and Onwudiwe, D. C. Graphitic carbon nitride-based catalysts and their applications: A review. *Nano-Structures & Nano-Objects*, 24:100577, 2020.

[11] (a) Zhang, G., Zhang, M., Ye, X., Qiu, X., Lin, S., and Wang, X. Iodine modified carbon nitride semiconductors as visible light photocatalysts for hydrogen evolution. *Advanced Materials*, 26(5):805-809, 2014. (b) Ge, L., Han, C., Liu, J., and Li, Y. Enhanced visible light photocatalytic activity of novel

polymeric g-C_3N_4 loaded with Ag nanoparticles. *Applied Catalysis A: General*, 409:215-222, 2011. (c) Kumar, S., Surendar, T., Baruah, A., and Shanker, V. Synthesis of novel and stable g-C_3N_4/Ag_3PO_4 inorganic-organic hybrid nanocomposite photocatalyst and enhancement of photocatalytic activity under visible light. *Journal of Material Chemistry: A*, 1:5333-5340, 2013. (d) Sun, J. X., Yuan, Y. P., Qiu, L. G., Jiang, X., Xie, A. J., Shen, Y. H., and Zhu, J. F. Fabrication of composite photocatalyst g-C_3N_4–ZnO and enhancement of photocatalytic activity under visible light. *Dalton Transactions*, 41(22):6756-6763, 2012. (e) Cui, Y., Huang, J., Fu, X., and Wang, X. Metal-free photocatalytic degradation of 4-chlorophenol in water by mesoporous carbon nitride semiconductors. *Catalysis Science & Technology*, 2(7):1396-1402, 2012. (f) Hong, J., Xia, X., Wang, Y., and Xu, R. Mesoporous carbon nitride with *in situ* sulfur doping for enhanced photocatalytic hydrogen evolution from water under visible light. *Journal of Materials Chemistry*, 22(30):15006-15012, 2012.

[12] (a) Yan, S. C., Li, Z. S., and Zou, Z. G. Photodegradation of rhodamine B and methyl orange over boron-doped g-C_3N_4 under visible light irradiation. *Langmuir*, 26(6):3894-3901, 2010. (b) Zhang, Y., Pan, Q., Chai, G., Liang, M., Dong, G., Zhang, Q., and Qiu, J. Synthesis and luminescence mechanism of multicolor-emitting g-C_3N_4 nanopowders by low temperature thermal condensation of melamine. *Scientific Reports*, 3(1):1-8, 2013.

[13] (a) Shi, L., Liang, L., Wang, F., Liu, M., Chen, K., Sun, K., Zhang, N., and Sun, J. Higher yield urea-derived polymeric graphitic carbon nitride with mesoporous structure and superior visible-light-responsive activity. *ACS Sustainable Chemistry & Engineering*, 3(12):3412-3419, 2015. (b) Kumar, A., Sharma, S. K., Sharma, G., Naushad, M., and Stadler, F. J. CeO_2/g-C_3N_4/V_2O_5 ternary nano hetero-structures decorated with CQDs for enhanced photo-reduction capabilities under different light sources: Dual Z-scheme mechanism. *Journal of Alloys and Compounds*, 838:155692, 2020.

[14] Zhang, G., Zhang, J., Zhang, M., and Wang, X. Polycondensation of thiourea into carbon nitride semiconductors as visible light photocatalysts. *Journal of Materials Chemistry*, 22(16):8083-8091, 2012.

[15] (a) Wang, X., Maeda, K., Thomas, A., Takanabe, K., Xin, G., Carlsson, J. M., Domen, K., and Antonietti, M. A metal-free polymeric photocatalyst for hydrogen production from water under visible light. *Nature Materials*, 8(1):76-80, 2009. (b) Takanabe, K., Kamata, K., Wang, X., Antonietti, M., Kubota, J., and Domen, K. Photocatalytic hydrogen evolution on dye-sensitized mesoporous carbon nitride photocatalyst with magnesium phthalocyanine. *Physical Chemistry Chemical Physics*, 12(40):13020-13025, 2010.

[16] Zhang, J., Zhang, M., Sun, R. Q., and Wang, X. A facile band alignment of polymeric carbon nitride semiconductors to construct isotype heterojunctions. *Angewandte Chemie International Edition*, 51(40):10145-10149, 2012.

[17] Kang, S., He, M., Chen, M., Wang, J., Zheng, L., Chang, X., Duan, H., Sun, D., Dong, M., and Cui, L. Ultrafast plasma immersion strategy for rational modulation of oxygen-containing and amino groups in graphitic carbon nitride. *Carbon*, 159:51-64, 2020.

[18] (a) Zhang, S., Li, J., Zeng, M., Zhao, G., Xu, J., Hu, W., and Wang, X. *In situ* synthesis of water-soluble magnetic graphitic carbon nitride photocatalyst and its synergistic catalytic performance. *ACS Applied Materials & Interfaces*, 5(23):12735-12743, 2013. (b) Kumar, R., Barakat, M. A., and Alseroury, F. A. Oxidized g-C_3N_4/polyaniline nanofiber composite for the selective removal of hexavalent chromium. *Scientific Reports*, 7(1):1-11, 2017. (c) Zhong, R., Zhang, Z., Yi, H., Zeng, L., Tang, C., Huang, L., and Gu, M. Covalently bonded 2D/2D Og-C_3N_4/TiO_2 heterojunction for enhanced visible-light photocatalytic hydrogen evolution. *Applied Catalysis B: Environmental*, 237:1130-1138, 2018. (d) Wang, H., Jiang, S., Chen, S., Li, D., Zhang, X., Shao, W., Sun, X., Xie, J., Zhao, Z., Zhang, Q., and Tian, Y. Enhanced singlet oxygen generation in oxidized graphitic carbon nitride for organic synthesis. *Advanced Materials*, 28(32):6940-6945, 2016. (e) Qiu, P., Xu, C., Chen, H., Jiang, F., Wang, X., Lu, R., and Zhang, X. One step synthesis of oxygen doped porous graphitic carbon nitride with remarkable improvement

of photo-oxidation activity: role of oxygen on visible light photocatalytic activity. *Applied Catalysis B: Environmental*, 206:319-327, 2017.

[19] Sun, J., Fu, Y., He, G., Sun, X., and Wang, X. Green Suzuki–Miyaura coupling reaction catalyzed by palladium nanoparticles supported on graphitic carbon nitride. *Applied Catalysis B: Environmental*, 165:661-667, 2015.

[20] Li, X. H., Baar, M., Blechert, S., and Antonietti, M. Facilitating room-temperature Suzuki coupling reaction with light: Mott-Schottky photocatalyst for C-C-coupling. *Scientific Reports*, 3(1):1-6, 2013.

[21] Choudhary, P., Bahuguna, A., Kumar, A., Dhankhar, S. S., Nagaraja, C. M., and Krishnan, V. Oxidized graphitic carbon nitride as a sustainable metal-free catalyst for hydrogen transfer reactions under mild conditions. *Green Chemistry*, 22(15):5084-5095, 2020.

[22] Wang, H., Jiang, S., Chen, S., Li, D., Zhang, X., Shao, W., Sun, X., Xie, J., Zhao, Z., Zhang, Q., and Tian, Y. Enhanced singlet oxygen generation in oxidized graphitic carbon nitride for organic synthesis. *Advanced Materials*, 28(32):6940-6945, 2016.

[23] Hak, C. H., Sim, L. C., Leong, K. H., Lim, P. F., Chin, Y. H., and Saravanan, P. M/g-C_3N_4 (M = Ag, Au, and Pd) composite: synthesis *via* sunlight photodeposition and application towards the degradation of bisphenol A. *Environmental Science and Pollution Research*, 25(25):25401-25412, 2018.

[24] (a) Cao, S., Li, Y., Zhu, B., Jaroniec, M., and Yu, J. Facet effect of Pd co-catalyst on photocatalytic CO_2 reduction over g-C_3N_4. *Journal of Catalysis*, 349:208-217, 2017. (b) Ma, J., Yang, Q., Wen, Y., and Liu, W. Fe-g-C_3N_4/graphitized mesoporous carbon composite as an effective Fenton-like catalyst in a wide pH range. *Applied Catalysis B: Environmental*, 201:232-240, 2017.

[25] Smýkalová, A., Foniok, K., Cvejn, D., Górecki, K. M., and Praus, P. The role of guanidine hydrochloride in graphitic carbon nitride synthesis. *Scientific Reports*, 11(1):1-18, 2021.

[26] (a) Dewan, A., Sarmah, M., Bharali, P., Thakur, A. J., Boruah, P. K., Das, M. R., and Bora, U. Pd nanoparticles-loaded honeycomb-structured bio-nanocellulose as a heterogeneous catalyst for heteroaryl cross-coupling reaction. *ACS Sustainable Chemistry & Engineering*, 9(2):954-966, 2021. (b) Verma, S., Baig, R. N., Nadagouda, M. N., and Varma, R. S. Photocatalytic C-H activation and oxidative esterification using Pd@ g-C_3N_4. *Catalysis Today*, 309:248-252, 2018.